Journal of Computational and Applied Mathematics 265 (2014) 120–138

Contents lists available at ScienceDirect

Journal of Computational and Applied Mathematics

journal homepage: www.elsevier.com/locate/cam

Comparisons between reduced order models and full 3D models for fluid–structure interaction problems in haemodynamics

C.M. Colciago [a,*], S. Deparis [a], A. Quarteroni [a,b]

[a] CMCS, Chair of Modelling and Scientific Computing, MATHICSE, Mathematics Institute of Computational Science and Engineering, EPFL, École Polytechnique Fédérale de Lausanne, Station 8, CH-1015 Lausanne, Switzerland

[b] MOX, Modeling and Scientific Computing, Department of Mathematics, Politecnico di Milano, Via Bonardi 9, Milan, Italy

ARTICLE INFO

Article history:
Received 2 December 2012
Received in revised form 13 March 2013

This paper is dedicated to Professor Ben-yu Guo on the occasion of his 70th birthday

Keywords:
Fluid–structure interaction
Transpiration conditions
Reduced order FSI models
Coupled momentum method
Haemodynamical applications
Navier–Stokes equations

ABSTRACT

When modelling the cardiovascular system, the effect of the vessel wall on the blood flow has great relevance. Arterial vessels are complex living tissues and three-dimensional specific models have been proposed to represent their behaviour. The numerical simulation of the 3D–3D Fluid–Structure Interaction (FSI) coupled problem has high computational costs in terms of required time and memory storage. Even if many possible solutions have been explored to speed up the resolution of such problem, we are far from having a 3D–3D FSI model that can be solved quickly.

In 3D–3D FSI models two of the main sources of complexity are represented by the domain motion and the coupling between the fluid and the structural part. Nevertheless, in many cases, we are interested in the blood flow dynamics in compliant vessels, whereas the displacement of the domain is small and the structure dynamics is less relevant. In these situations, techniques to reduce the complexity of the problem can be used. One consists in using transpiration conditions for the fluid model as surrogate for the wall displacement, thus allowing problem's solution on a fixed domain. Another strategy consists in modelling the arterial wall as a thin membrane under specific assumptions (Figueroa et al., 2006, Nobile and Vergara, 2008) instead of using a more realistic (but more computationally intensive) 3D elastodynamic model. Using this strategy the dynamics of the vessel motion is embedded in the equation for the blood flow. Combining the transpiration conditions with the membrane model assumption, we obtain an attractive formulation, in fact, instead of solving two different models on two moving physical domains, we solve only a Navier–Stokes system in a fixed fluid domain where the structure model is integrated as a generalized Robin condition. In this paper, we present a general formulation in the boundary conditions which is independent of the time discretization scheme choice and on the stress–strain constitutive relation adopted for the vessel wall structure.

Our aim is, first, to write a formulation of a reduced order model with zero order transpiration conditions for a generic time discretization scheme, then to compare a 3D–3D FSI model and a reduced FSI one in two realistic patient-specific cases: a femoropopliteal bypass and an aorta. In particular, we are interested in comparing the wall shear stresses, in fact this quantity can be used as a risk factor for some pathologies such as atherosclerosis or thrombogenesis. More in general we want to assess the accuracy and the computational convenience to use simpler formulations based on reduced order models. In particular, we show that, in the case of small displacements, using a 3D–3D FSI linear elastic model or the correspondent reduced order one yields many similar results.

* Corresponding author. Tel.: +41 21 69 35509.
E-mail addresses: claudia.colciago@epfl.ch (C.M. Colciago), simone.deparis@epfl.ch (S. Deparis), alfio.quarteroni@epfl.ch (A. Quarteroni).

0377-0427/$ – see front matter © 2013 Elsevier B.V. All rights reserved.
http://dx.doi.org/10.1016/j.cam.2013.09.049

1. Introduction

Cardiovascular diseases, such as atherosclerosis, thrombogenesis and heart failure, have a great relevance in the current biomedical research since they are responsible for more than a half mortality in the developed countries [1,2]. Medical doctors need to better understand the biophysical processes in order to identify the risk factors, to predict the possible scenarios, and, hopefully, to find suitable therapies.

The cardiovascular system is composed by a network of vessels in which blood flows under the stimuli of a periodic pump, the heart. Arterial and vein vessels are not just inert pipes that convey the blood to all the organs of the body, they are complex living tissues that interact with the flow and adapt depending on several factors. Another source of complexity in the cardiovascular system is the variability of geometries and physical properties of vessels in the human body.

We can observe a great variability of these features during the heart cycle and, moreover, among different individuals, depending on the age, life-quality or genetics. In fact, the complexity of the cardiovascular system makes impossible an *a priori* and generic prediction of the physical behaviour and risk factors and highlights the importance of finding a way to simulate these phenomena using a subject-specific approach.

Blood flow in large vessels can be considered as an incompressible fluid [2,1]. Even if at low shear rate the blood shows a non-Newtonian behaviour (for example particles tend to form aggregates), in large arteries with diameter larger than 0.3 cm, it is widely accepted to assume a Newtonian behaviour. Since we deal with large vessels such as the aorta (about 3 cm diameter) or femoral arteries (about 0.5 cm diameter), this approximation is justified [2].

When modelling the cardiovascular system we also have to account for the coupling between the solid and the fluid part. The interactions among blood, vessels, and organs can occur at different levels, such as chemical reactions, mechanotransduction of signals or drug delivery. Experiments show that many risk factors are strictly linked to the mechanical stimuli such as stress exchange between blood flow and vessel wall. The research in numerical analysis has therefore produced a great effort in the modelling of the cardiovascular dynamics. Depending on the specific application a well-suited formulation of the equations can be written. For example, if we are interested to averaged *macroscopic* quantities such as mean flows or pressures in arteries, we can rely on one-dimensional networks as the ones proposed in [3,4]. If the goal is the distribution of the stresses inside the thickness of the wall, three-dimensional specific models are required for the structure. Several structural models for the arterial wall have been proposed [1] but there is still no evidence on which constitutive relation is better suited for the vessel wall mechanics. The numerical simulation of the coupled problem has high computational costs in terms of required time and memory. Many possible solutions have been explored to speed up the resolution of such problem [5–11], nevertheless, we are far from having a 3D–3D fluid–structure interaction model that can be solved quickly.

Most applications are focused on modelling the effect of the structure on the blood motion or on the exchange of mechanical stresses, as well as the localization of high shear stresses or high vorticity zones. Those factors are linked to pathologies like atherosclerosis or thrombogenesis. In numerous situations, *reduced* order structural models can be used, where the effect of the wall is *reduced* to a thin membrane under specific assumptions.

A Koiter linear elastic shell model for the vessel wall is used for example in [12–14], where the displacement is considered non zero only in the normal direction and the model is solved on a cylindrical geometry. In particular in [13–15], suitable explicit and kinematically coupling algorithms are used to solve the equations, the same type of algorithm is used in [16], where a Koiter viscoelastic shell model on a cylindrical geometry with longitudinal displacement is considered. Explicit and kinematically coupled schemes are analyzed in [17]. Implicit coupling algorithms are instead used in [12,18,19] where the dynamics of the vessel motion is directly embedded in the equation for the blood flow. In particular, in [18,19], also realistic applications are discussed but no direct comparison with a 3D–3D FSI model is developed. The main advantage is that a simpler formulation is generated, where the dynamics of vessel motion is directly embedded in the equation for the blood flow. Moreover, instead of solving two different models on different computational domains (fluid and solid, respectively), we solve only a Navier–Stokes system in the fluid domain. This formulation is also suitable to be used in other numerical contexts such as optimization and control analysis [20–23].

Usually FSI problems are solved on a specific portion of a vessel. The region of interest is for example the proximity of an anastomosis, a bifurcation, or a tract of the aorta, either in physiological or pathological conditions. The aim of this work is to compare the 3D–3D FSI model with a reduced order one in two different real cases: blood flow in a femoropopliteal bypass and blood flow in the aorta in healthy conditions. In the first case we analyse a segment of the bypass near to the anastomosis between the graft and the femoral artery. We are interested in studying the distribution of the wall shear stress after the anastomosis in order to see if they recover the physiological range. We then consider the geometry of an aorta (from the ascending aorta to the abdominal aorta with the principal branches) featuring physiological conditions. In the case of the femoropopliteal bypass the wall displacement is moderate and we expect that the reduced order model is closed to the 3D–3D FSI one; while in the case of the aorta the wall displacement is much larger and we would like to measure how far the reduced model stands from the 3D–3D FSI one. Our comparison will focus on output of interest, in particular, the wall shear stress at the fluid–structure interface.

In the following sections we present the standard equations of an FSI model and the application of transpiration conditions [6] which will allow us to make our computations on a steady domain with a fixed mesh. In Section 2 we present two reduced structural models: an inertial–algebraic model [12] and a membrane model that, coupled with the fluid equations, arises in the so called coupled momentum method [18]. In Section 3 we report the results on three cases: a simple cylinder,

a femoropopliteal bypass, and an aorta. In the first case we compare the results with those in [18]. In the second and the third case we make a comparison between a reduced order FSI model and a truly 3D–3D FSI one.

2. 3D–3D fluid–structure interaction model

2.1. Fluid and structure equations

The domain under consideration is composed of a fluid and a compliant structure (see Fig. 1). The reference configuration and all the variables defined on this domain are addressed with a *hat* $\widehat{\cdot}$. The model is described by Navier–Stokes equations for the fluid, that are coupled with a linear elastic St. Venant–Kirchhoff model for the structure. The physical unknowns of the system are the fluid velocity $\mathbf{u}$ and the pressure p, expressed in the current configuration, and the solid displacement $\widehat{\mathbf{d}}_s$, usually computed on the reference configuration.

Some information at the boundaries are required to solve the problems and compute the unknowns of the simulations. At the inlet and outlet boundaries, data about mean quantities, such as pressure or flows of the vessel, are given. These quantities as well as the fluid equations are referred to an Eulerian frame of reference, in fact they are measured on a specific fixed section of the space. In contrast, the structure model is usually written in a Lagrangian formulation, which consists in following the material particle during the evolution of time. Thus, it can be useful to treat the interface between fluid and solid with a material frame of reference. To deal with this hybrid treatment of the boundary conditions, an Arbitrary Lagrangian Eulerian (ALE) formulation for the fluid equations has been proposed and analyzed [24,25]. The ALE formulation of the coupled problem yields an *artificial* variable, the fluid domain displacement $\widehat{\mathbf{d}}_f$, which helps ensuring that the fluid domain follows the material particles of the vessel wall at the interface Γ. By means of $\widehat{\mathbf{d}}_f$, it is possible to introduce the Arbitrary Lagrangian Eulerian (*ALE*) map $\mathcal{A}_t$ that, at each time t, maps the reference fluid domain $\widehat{\Omega}_f$ in the current computational domain $\Omega_f(t)$:

$$\begin{aligned} &\mathcal{A}_t : \widehat{\Omega} \to \Omega_f(t) \\ &\widehat{\mathbf{x}} \mapsto \mathcal{A}_t(\widehat{\mathbf{x}}) = \widehat{\mathbf{x}} + \widehat{\mathbf{d}}_f(\widehat{\mathbf{x}}). \end{aligned} \tag{1}$$

Let $\mathbf{w}$ be the time derivative of the ALE map:

$$\mathbf{w}(\mathcal{A}_t(\widehat{\mathbf{x}})) = \left.\frac{\partial \mathcal{A}_t}{\partial t}\right|_{\widehat{\mathbf{x}}} = \left.\frac{\partial \widehat{\mathbf{d}}_f}{\partial t}\right|_{\widehat{\mathbf{x}}}. \tag{2}$$

The Navier–Stokes equations for the fluid motion of the blood written in the ALE formulation read as follows:

$$\begin{cases} \rho_f \left.\dfrac{\partial \mathbf{u}}{\partial t}\right|_{\hat{x}} - \nabla_x \cdot \sigma_f(\mathbf{u}, p) + \rho_f((\mathbf{u} - \mathbf{w}) \cdot \nabla_x)\mathbf{u} = \mathbf{f}_f & \text{in } \Omega_f(t) \times (0, T), \\ \nabla_x \cdot \mathbf{u} = 0 & \text{in } \Omega_f(t) \times (0, T), \\ \mathbf{u}|_{t=0} = \mathbf{u}_0 & \text{in } \Omega_f(0), \\ \mathbf{u} = \mathbf{g} & \text{in } \Gamma_D^f \times (0, T), \\ \sigma_f \mathbf{n} = \mathbf{h} & \text{in } \Gamma_N^f \times (0, T), \end{cases} \tag{3}$$

where $\mathbf{g}$, $\mathbf{h}$ and $\mathbf{u}_0$ are given functions, $\sigma_f(\mathbf{u}, p)$ is the Cauchy stress tensor

$$\sigma_f(\mathbf{u}, p) = \mu(\nabla_x \mathbf{u} + (\nabla_x \mathbf{u})^T) - pI, \tag{4}$$

and, referring to Fig. 1, $\Gamma_N^f \cup \Gamma_D^f = \Gamma_{\text{in}}(t) \cup \Gamma_{\text{out}}(t)$. This model has to be completed by suitable coupling conditions on the interface Γ. Before introducing these conditions, we introduce the solid equations that govern the vessel motion. The vessel tissue is a living multi-component organ with anisotropic, non-linear properties. We consider a linear isotropic St. Venant–Kirchhoff model, other models for the vessel wall can be founded in [1]. The equations for the solid displacement written in a Lagrangian framework read

$$\begin{cases} \rho_s \dfrac{\partial^2 \widehat{\mathbf{d}}_s}{\partial t^2} - \nabla_{\hat{x}} \cdot \mathbf{\Pi} = \widehat{\mathbf{f}}_s & \text{in } \widehat{\Omega}_s \times (0, T), \\ \widehat{\mathbf{d}}_s = \mathbf{0} & \text{on } \widehat{\Gamma}_{\text{in}}^s \cup \widehat{\Gamma}_{\text{out}}^s \times (0, T), \\ \widehat{\mathbf{d}}_s|_{t=0} = \widehat{\mathbf{d}}_s^0 & \text{in } \widehat{\Omega}_s, \\ \left.\dfrac{\partial \widehat{\mathbf{d}}_s}{\partial t}\right|_{t=0} = \widehat{\mathbf{d}}_s^v & \text{in } \widehat{\Omega}_s, \end{cases} \tag{5}$$

where ρ_s is the density of the vessel wall material and

$$\mathbf{\Pi} = \lambda \operatorname{tr}(\epsilon) + 2\mu_s \epsilon \tag{6}$$

is the first Piola–Kirchhoff stress tensor, with $\epsilon = \frac{(\nabla_{\hat{x}} \widehat{\mathbf{d}}_s + (\nabla_{\hat{x}} \widehat{\mathbf{d}}_s)^T)}{2}$, and λ and μ_s are, respectively, the first and the second Lamé coefficients defining the characteristic of the material. In the St. Venant–Kirchhoff model, those two coefficients are related

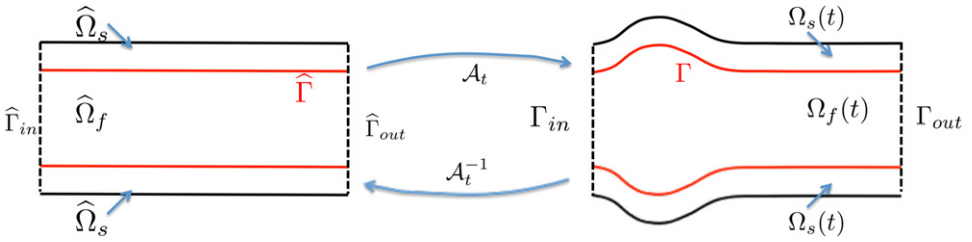

Fig. 1. Geometrical configuration.

with the Young modulus E and the Poisson ν ratio as follows:

$$\lambda = \frac{E\nu}{(1-2\nu)(1+\nu)} \quad \text{and} \quad \mu_s = \frac{E}{2(1+\nu)}. \tag{7}$$

An equation for the fluid domain displacement is also required. This quantity can be computed in an arbitrary way and a widely adopted method is to compute the displacement $\widehat{\mathbf{d}}_f$ as an harmonic extension of the interface displacement $\widehat{\mathbf{d}}_s|_{\widehat{\Gamma}}$:

$$\begin{cases} \triangle\widehat{\mathbf{d}}_f = 0 & \text{in } \widehat{\Omega}_f, \\ \widehat{\mathbf{d}}_f = \widehat{\mathbf{d}}_s & \text{on } \widehat{\Gamma}, \\ \widehat{\mathbf{d}}_f = \mathbf{0} & \text{on } \widehat{\Gamma}^f_{\text{in}} \cup \widehat{\Gamma}^f_{\text{out}}. \end{cases} \tag{8}$$

At the discrete level, we need to ensure that the transformation of the domain due to $\widehat{\mathbf{d}}_f$ is admissible. For this reason, at each time step, the measure of finite element tetrahedra should remain positive after having *moved* the fluid mesh according to the displacement $\widehat{\mathbf{d}}_f$.

2.2. Coupling conditions

Suitable coupling conditions at the fluid–structure interface $\widehat{\Gamma}$ close the system:

- kinematic condition: the continuity of the fluid and the solid particle velocity

$$\frac{\partial\widehat{\mathbf{d}}_s}{\partial t} = \mathbf{u} \circ \mathcal{A}_t \quad \text{on } \widehat{\Gamma}; \tag{9}$$

- dynamic condition: the continuity of the normal stresses

$$J_f \sigma_f F_f^{-T} \widehat{\mathbf{n}} = \boldsymbol{\Pi}\widehat{\mathbf{n}} \quad \text{on } \widehat{\Gamma}, \tag{10}$$

  where $\widehat{\mathbf{n}}$ is the outward normal to the fluid reference domain, F_f is the deformation gradient computed as $F_f = I + \nabla_{\hat{x}}\widehat{\mathbf{d}}_f$ and J_f its determinant;
- the geometry adherence

$$\widehat{\mathbf{d}}_s = \widehat{\mathbf{d}}_f \quad \text{on } \widehat{\Gamma} \tag{11}$$

  expresses a condition which ensures that the fluid domain sticks to the structure.

This coupled FSI problem is discretized by 3D finite elements in space and a geometry-convective time discretization. The fluid convective term is treated semi-implicitly and the domain geometry is recovered from the previous time step through suitable extrapolations [26]. At each time step a single large linear system has to be solved. Suitable parallel preconditioners, based on domain decomposition techniques, are employed to speed up the resolution of the linear system. More details can be found in [27].

3. Reduced order fluid–structure interaction models

Under specific assumptions, it is possible to achieve a reduced formulation for the FSI problem. We focus on two difficulties that arise when dealing with FSI problems and we introduce some hypotheses that allow us to retrieve a simpler formulation. First, we focus on the complexity due to the moving domain, which, in the numerical resolution, requires the update of the mesh and the re-computation of the matrices at each time step. Assuming that the wall displacement is small, we linearized the domain movement using transpiration conditions [6] and we write the equations on a fixed geometry. The second source of complexity is the coupling between the fluid and the solid problem. Instead of adopting a 3D elastodynamic model for the structural part, the vessel is modelled as a membrane and embedded as a boundary condition for the fluid equation. The resulting model is in fact a Navier–Stokes problem on a steady domain with a generalized Robin boundary condition on the interface Γ.

In this section we formalize the reduced models that were introduced in [12,18]. The goal is to investigate, in specific clinical cases, how these reductions affect the result of the simulations.

3.1. Transpiration conditions

In the fully 3D–3D FSI model with linear elasticity there are two sources of non-linearity: the first one is due to the fluid convective term (which is quadratic in the unknown velocity $\mathbf{u}$), the second is due to the moving fluid geometry that adheres to the structure. At the discrete level, the mesh movement implies the re-computation of the finite element matrices at each time step. To reduce the computational time, suitable transpiration conditions can be introduced that allow to work with a fixed fluid domain, see [6]. This hypothesis does not affect the results of the simulation if the displacement of the physical domain is small enough.

We use Taylor series to expand the velocity field $\mathbf{u}$ in a neighbourhood of a point of the interface $\widehat{\Gamma}$. Eq. (3) is then written on a fixed domain, thus getting rid of one source of non-linearity and saving computational time by assembling the finite element matrices only once for the entire simulation. The Taylor expansion for the fluid velocity reads

$$\begin{aligned}\mathbf{u}(\mathcal{A}_t(\widehat{\mathbf{x}})) &= \mathbf{u}(\widehat{\mathbf{x}}) + \nabla_{\widehat{x}}\mathbf{u}|_{\widehat{\mathbf{x}}}(\mathcal{A}_t(\widehat{\mathbf{x}}) - \widehat{\mathbf{x}}) + O(\|(\mathcal{A}_t(\widehat{\mathbf{x}}) - \widehat{\mathbf{x}})\|^2)\\ &= \mathbf{u}(\widehat{\mathbf{x}}) + \nabla_{\widehat{x}}\mathbf{u}|_{\widehat{\mathbf{x}}}\widehat{\mathbf{d}}_f + O(\|\widehat{\mathbf{d}}_f|_{\widehat{\Gamma}}\|^2) \quad \text{on } \widehat{\Gamma}. \end{aligned} \tag{12}$$

An even simpler version is a zero order extrapolation, namely:

$$\mathbf{u}(\mathcal{A}_t(\widehat{\mathbf{x}})) = \mathbf{u}(\widehat{\mathbf{x}}) + O(\|\widehat{\mathbf{d}}_f|_{\widehat{\Gamma}}\|) \quad \text{on } \widehat{\Gamma}. \tag{13}$$

Using the geometric adherence condition, it is possible to write this relation only in function of $\mathbf{u}$ and $\widehat{\mathbf{d}}_s$:

$$\mathbf{u}(\mathcal{A}_t(\widehat{\mathbf{x}})) = \mathbf{u}(\widehat{\mathbf{x}}) + O(\|\widehat{\mathbf{d}}_s|_{\widehat{\Gamma}}\|). \tag{14}$$

This equation allows us to express all the quantities on the reference configuration $\widehat{\Omega}$. The coupling conditions can be re-written with a simpler formulation:

$$\frac{\partial\widehat{\mathbf{d}}_s(\widehat{\mathbf{x}})}{\partial t} = \mathbf{u}(\widehat{\mathbf{x}}). \tag{15}$$

Similar Taylor expansion on the stresses $\sigma_f(\mathbf{u}, p)$ leads to:

$$\sigma_f(\mathcal{A}_t(\widehat{\mathbf{x}})) = \sigma_f(\widehat{\mathbf{x}}) + \nabla_{\widehat{x}}\sigma_f|_{\widehat{\mathbf{x}}}\widehat{\mathbf{d}}_s + O(\|\widehat{\mathbf{d}}_s|_{\widehat{\Gamma}}\|^2), \tag{16}$$

where, again, if we use zero order extrapolation, we obtain:

$$\sigma_f(\mathcal{A}_t(\widehat{\mathbf{x}})) = \sigma_f(\widehat{\mathbf{x}}) + O(\|\widehat{\mathbf{d}}_s|_{\widehat{\Gamma}}\|) \approx \sigma_f(\widehat{\mathbf{x}}). \tag{17}$$

The coupling condition for the continuity of the stresses on the interface $\widehat{\Gamma}$ reads:

$$J_f\sigma_f(\widehat{\mathbf{x}})F_s^{-T}\widehat{\mathbf{n}} = \boldsymbol{\Pi}(\widehat{\mathbf{d}}_s)\widehat{\mathbf{n}}. \tag{18}$$

The geometric adherence is replaced by the transpiration condition (15) and the resolution of the problem for the fluid domain displacement $\widehat{\mathbf{d}}_f$ is no more required. In fact, if we perform the Taylor expansion on the ALE map itself, we obtain:

$$\mathcal{A}_t(\widehat{\mathbf{x}}) = \widehat{\mathbf{x}} + \nabla_{\widehat{x}}\mathcal{A}_t(\widehat{\mathbf{x}})|_{\widehat{\mathbf{x}}}(\mathcal{A}_t(\widehat{\mathbf{x}}) - \widehat{\mathbf{x}}) + O(\|\widehat{\mathbf{d}}_s|_{\widehat{\Gamma}}\|^2).$$

If a zero order transpiration condition is used, it holds

$$\mathcal{A}_t(\widehat{\mathbf{x}}) = \widehat{\mathbf{x}} \quad \text{whence } F_f = I.$$

The condition on the normal stresses (18) is then replaced by the following one

$$\big(\sigma_f(\widehat{\mathbf{x}})\big)\widehat{\mathbf{n}} = \boldsymbol{\Pi}(\widehat{\mathbf{d}}_s)\widehat{\mathbf{n}} \quad \text{on } \widehat{\Gamma}. \tag{19}$$

The fluid domain is now fixed and all the operations are performed on the domain $\widehat{\Omega}$. In what follows, to simplify the notation, we remove the $\widehat{\cdot}$ from all the variables.

To write the weak formulation of the FSI problem with zero order transpiration condition, we introduce the following functional spaces:

$$\mathbf{V}_f = \{\mathbf{v} \in [H^1(\Omega_f)]^d : \mathbf{v}|_{\Gamma_D^f} = \mathbf{g}\} \tag{20}$$

$$\mathbf{V}_f^0 = \{\mathbf{v} \in [H^1(\Omega_f)]^d : \mathbf{v}|_{\Gamma_D^f} = \mathbf{0}\} \tag{21}$$

$$\mathbf{V}_s = \{\mathbf{v}_s \in [H^1(\Omega_s)]^d : \mathbf{v}_s|_{\Gamma_{\text{in}}^s \cup \Gamma_{\text{out}}^s} = \mathbf{0}\} \tag{22}$$

$$M = L^2(\Omega_f) \tag{23}$$

where d is the space dimension of the problem at hand. Then, the weak formulation reads:

find $(\mathbf{u}, p, \mathbf{d}_s) \in L^2(0,T;\mathbf{V}_f) \cap C^0(0,T;L^2(\Omega)) \times L^2(0,T;M) \times H^1(0,T;\mathbf{V}_s)$
with $\mathbf{u}|_{t=0} = \mathbf{u}_0 \in \mathbf{V}_f$ and $\mathbf{d}_s|_{t=0} = \mathbf{d}_0 \in \mathbf{V}_s$ such that for all $t \in (0,T]$:

$$\begin{aligned}
&\int_{\Omega_f} \rho_f \left(\frac{\partial \mathbf{u}}{\partial t} + (\mathbf{u}\cdot\nabla_x)\mathbf{u} \right) \cdot \mathbf{v}_f d\Omega_f + \int_{\Omega_f} \left(\mu(\nabla_x \mathbf{u} + \nabla_x^T \mathbf{u}) : \nabla_x \mathbf{v}_f - p\nabla_x \cdot \mathbf{v}_f \right) d\Omega_f \\
&\quad + \int_{\Omega_s} \rho_s \frac{\partial^2 \mathbf{d}_s}{\partial t^2} \cdot \mathbf{v}_s d\Omega_s + \int_{\Omega_s} \mathbf{\Pi}(\mathbf{d}_s) : \nabla_x \mathbf{v}_s d\Omega_s \\
&\quad = \int_{\Omega_f} \mathbf{f}_f \cdot \mathbf{v}_f d\Omega_f + \int_{\Gamma_N} \mathbf{h} \cdot \mathbf{v}_f d\Gamma \\
&\int_{\Omega_f} q \nabla_x \cdot \mathbf{u} d\Omega_f = 0 \\
&\frac{\partial \mathbf{d}_s}{\partial t} = \mathbf{u} \quad \text{on } \Gamma \qquad\qquad \forall (\mathbf{v}_f, q, \mathbf{v}_s) \in \mathbf{V}_f^0 \times M \times \mathbf{V}_s.
\end{aligned} \tag{24}$$

3.2. A first reduced structural model: inertial–algebraic model

Another source of complexity in an FSI problem is indeed the coupling between the fluid and the structural models. When we model the vessel wall as a membrane, suitable coupling technique can be used in order to embed the structural model in the fluid system as a boundary condition. The first reduced structural model that we are going to present is the *inertial–algebraic model* and it was proposed in [12]. It is based on a Koiter model under the assumption of small deformations and negligible bending terms. Furthermore, the vessel is considered as an isotropic–homogeneous material and a linear constitutive stress–strain relation is used. The thickness of the wall is supposed to be constant in space.

Let us assume that the interface position Γ of the membrane can be identified by a regular mapping with a two-dimensional plain set ω. We denote with $E^{\alpha\beta\lambda\delta}$ the stress tensor written in the domain ω, where we used the Greek letters for indices taking their values in the set $\{1, 2\}$. Moreover, we introduce the symbol $\gamma_{\alpha\beta}(\mathbf{d}_s)$ to address the change of metric when passing from the domain ω to the surface Γ. The weak formulation of the Koiter's equation reads:

$$\int_\Gamma \rho_s h_s \frac{\partial^2 \mathbf{d}_s}{\partial t^2} \cdot \mathbf{v}_s + \int_\Gamma h_s E^{\alpha\beta\lambda\delta} \gamma_{\alpha\beta}(\mathbf{d}_s)\gamma_{\lambda\delta}(\mathbf{v}_s) d\gamma = \int_\Gamma \mathbf{f}_s \cdot \mathbf{v}_s \quad \forall \mathbf{v}_s \in V_s. \tag{25}$$

Using the above mentioned assumptions and adding the hypothesis that the displacement is non zero only in the normal direction, the contribution of the stresses can be simplified as:

$$E^{\alpha\beta\lambda\delta}\gamma_{\alpha\beta}(\mathbf{d}_s)\gamma_{\lambda\delta}(\mathbf{v}_s) = \frac{h_s E}{1-\nu^2}(4\rho_1^2 - 2(1-\nu)\rho_2)(\mathbf{d}_s \cdot \mathbf{n})(\mathbf{v}_s \cdot \mathbf{n}), \tag{26}$$

where E is the Young modulus, ν the Poisson coefficient, h_s the wall thickness, and ρ_1 and ρ_2 are the mean and the Gaussian curvature, respectively. The corresponding strong formulation of the Eq. (25) is then reduced to an ordinary differential scalar problem. We denote by

$$d = \mathbf{d}_s \cdot \mathbf{n}$$

the normal displacement of the membrane wall and, at each point $\mathbf{x} \in \Gamma$, $\mathbf{n}$ represents the normal unit vector on the interface. Then, the strong formulation of the inertial–algebraic model reads:

$$\rho_s h_s \frac{\partial^2 d}{\partial t^2} + \beta d = f_s \quad \text{on } \Gamma \times (0,T), \tag{27}$$

where f_s is a given (scalar) forcing term and

$$\beta = \frac{h_s E}{1-\nu^2}(4\rho_1^2 - 2(1-\nu)\rho_2). \tag{28}$$

Due to the previous normal displacement assumption, the coupling at the interface Γ takes into account only the normal component of the velocities and of the stresses. This translates into the constraints:

$$\mathbf{u}\cdot\mathbf{n} = \frac{\partial d}{\partial t} \quad \text{on } \Gamma \quad \text{and} \quad f_s = -(\sigma_f \mathbf{n})\cdot\mathbf{n} \quad \text{on } \Gamma. \tag{29}$$

Homogeneous Dirichlet conditions enforced in the tangent directions close the problem. This is consistent with the null tangential displacement of the structure. We underline that in the coupling equations we drop the mapping terms from the reference to the current configuration thanks to the use of transpiration conditions of zero order. A more general formulation can be found in [12]. Using the coupling conditions, Eq. (27) can be written as a boundary condition on the interface Γ for

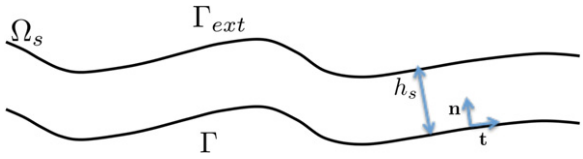

Fig. 2. Geometrical configuration of the wall.

the Navier–Stokes problem, we refer to [12] for the details. This process is mainly based on a finite difference discretization of the coupling condition on the continuity of the velocities.

Let us write down the boundary condition for the fluid problem derived from the structural equation. For the sake of simplicity, we suppose to use an Implicit Euler scheme and zero order transpiration conditions, nevertheless the result can be generalized to other kind of time discretization schemes. In the next section we will consider the general case and we will perform all the steps that, starting from the solid model equation, lead to a boundary condition for the fluid problem. Introducing the notation ϕ^n to address a generic quantity $\phi(t)$ at a fixed time $t = t_n$, using an Implicit Euler time discretization, and denoting Δt the time step, the discretization of the continuity of the normal velocity reads

$$d^{n+1} = \Delta t \mathbf{u}^{n+1} \cdot \mathbf{n} + d^n.$$

At a fixed time step t^{n+1}, the inertial–algebraic model equation (27) can be written ad follows:

$$\rho_s h_s \frac{\mathbf{u}^{n+1} \cdot \mathbf{n} - \mathbf{u}^n \cdot \mathbf{n}}{\Delta t} + \beta(\Delta t \mathbf{u}^{n+1} \cdot \mathbf{n} + d^n) = -(\sigma_f \mathbf{n}) \cdot \mathbf{n} \quad \text{on } \Gamma, \tag{30}$$

which is a Robin boundary condition in the normal direction for the fluid problem.

The coefficient β depends on the geometric curvature of the surface. This can represent a difficulty in a real application, where the geometry of the domain is generated starting from medical images. The surface meshes are composed by triangles and the curvature in a vertex is defined by considering a suitable average between the orientation of the triangles sharing that vertex. Due to the small irregularities of real vessels, the values of the curvatures can be subject to large variations that can affect the results of the simulations. One possible solution to this problem is to refine the mesh until β is smooth enough to avoid instabilities in the solution [28]. Nevertheless, this process can lead to meshes with a high number of tetrahedra and very small grid step. One could end up in solving ill-conditioned and computationally expensive problems that do not improve the accuracy of the solution and do not represent a real gain with respect to 3D–3D FSI problems with coarser meshes.

3.3. A second reduced structural model: membrane model

We discuss here another possible approach to reduce the equation of the structure to a membrane model, as proposed in [19,18]. The resulting fluid model with embedded structure was given the name *coupled momentum method*. Its formulation is detailed in [18] for a fluid–structure interaction problem with linear constitutive stress–strain relation for the structure, zero order transpiration conditions and generalized-α method for the time discretization. In this work we derive instead a general formulation which is independent of the time discretization scheme and the structural constitutive relation.

As in the inertial–algebraic model, also the coupled momentum method relies on the hypothesis of a linear elastic constitutive relation between the stress and the strain of the membrane. Moreover, the model is derived under the assumptions of homogeneous–isotropic material, thin-wall structure, and negligible bending terms. Differently form the previous model, the displacement is considered non zero in all the three space directions. An homogeneous distribution of the physical quantities in the radial direction inside the vessel wall is assumed. Also in this case the thickness of the wall is supposed constant.

The hypothesis of a thin-wall structure and of homogeneous radial stresses can be translated in the following mathematical relations. With respect to the notation of Fig. 2, let denote γ the coordinate aligned to the tangential versor $\mathbf{t}$ and η the coordinate aligned to the normal $\mathbf{n}$. Due to the homogeneous distribution along η, all the integrals in the domain Ω_s can be written as integrals on the interface Γ according to the relation

$$\int_{\Omega_s} \phi(\gamma, \eta) = \int_0^{h_s} d\eta \int_\Gamma \phi(\gamma) d\gamma = h_s \int_\Gamma \phi(\gamma) d\gamma, \tag{31}$$

and to set to zero all the derivatives in the normal direction:

$$\nabla_x \phi \cdot \mathbf{n} = 0.$$

Thus on Γ:

$$\nabla_x \phi = (\nabla_x \phi \cdot \mathbf{t})\mathbf{t} + (\nabla_x \phi \cdot \mathbf{n})\mathbf{n} = (\nabla_x \phi \cdot \mathbf{t})\mathbf{t}, \qquad \nabla_\gamma \phi := (\nabla_x \phi \cdot \mathbf{t})\mathbf{t}, \tag{32}$$

where we have introduced the symbol ∇_γ to denote the surface gradient on the interface Γ.

To derive a well-posed weak formulation of the problem on the interface Γ, the functional space $\mathbf{V}_s$ is restricted to ensure higher regularity on the boundary.

$$\mathbf{V}_s^{\Gamma} = \{\mathbf{v}_s \in \mathbf{V}_s : \mathbf{v}_s|_{\Gamma} \in H^1(\Gamma)\}. \tag{33}$$

Neglecting volumetric forces ($\mathbf{f}_s = \mathbf{0}$), the weak formulation of the problem (8) reads

$$\int_{\Omega_s} \rho_s \frac{\partial^2 \mathbf{d}_s}{\partial t^2} \cdot \mathbf{v}_s d\Omega_s + \int_{\Omega_s} \mathbf{\Pi}(\mathbf{d}_s) : \nabla_x \mathbf{v}_s d\Omega_s = \int_{\Gamma} \mathbf{\Pi}(\mathbf{d}_s)\mathbf{n}_{\text{ext}} \cdot \mathbf{v}_s d\Gamma, \tag{34}$$

where $\mathbf{n}_{\text{ext}}$ is the outward normal to the solid domain. Using (31), Eq. (34) reads

$$h_s \int_{\Gamma} \rho_s \frac{\partial^2 \mathbf{d}_s}{\partial t^2} \cdot \mathbf{v}_s d\Gamma + h_s \int_{\Gamma} \mathbf{\Pi}_{\gamma}(\mathbf{d}_s) : \nabla_{\gamma} \mathbf{v}_s d\Gamma = \int_{\Gamma} \mathbf{\Pi}_{\gamma}(\mathbf{d}_s)\mathbf{n}_{\text{ext}} \cdot \mathbf{v}_s d\Gamma. \tag{35}$$

Accordingly with the notation of (32), $\mathbf{\Pi}_{\gamma}(\phi)$ is the stress tensor of the structure applied to a generic quantity ϕ where just surface derivatives are involved. The expression of $\mathbf{\Pi}_{\gamma}(\phi)$ depends on the constitutive membrane model chosen for the vessel wall.

Let us introduce the notation for the discretization of the temporal derivatives. Our goal of this section is to write the coupled momentum method as introduced in [19,18] for a generic time discretization method. Given a generic quantity ϕ, we use the notation $\partial_t \phi$ to address the discretization of its first order time derivative and we split it into two terms as follows:

$$\left.\frac{\partial \phi}{\partial t}\right|_{t=t^{n+1}} \approx \partial_t \phi = \frac{\alpha}{\Delta t}\phi^{n+1} - f(\phi^n, \dot{\phi}^n, \ddot{\phi}^n). \tag{36}$$

Here $f_{\phi}^n = f(\phi^n, \dot{\phi}^n, \ddot{\phi}^n)$ is a function of known quantities and its formula is given by the specific discretization method that is chosen. Moreover, we use the following notation to address the discrete first order derivative in time of a generic quantity ϕ:

The discretization of the velocity coupling condition (15) reads:

$$\frac{\alpha}{\Delta t}\mathbf{d}_s^{n+1} = \mathbf{u}^{n+1} + f_{\mathbf{d}}^n. \tag{37}$$

Plugging the discretization of coupling condition (37) into $\mathbf{\Pi}_{\gamma}$, the following equation holds:

$$\mathbf{\Pi}_{\gamma}(\mathbf{d}_s^{n+1}) = \frac{\Delta t}{\alpha}(\mathbf{\Pi}_{\gamma}(\mathbf{u}^{n+1} + f_{\mathbf{d}}^n)). \tag{38}$$

If the constitutive stress–strain relation is linear, it is possible to write:

$$\mathbf{\Pi}_{\gamma}(\mathbf{d}_s^{n+1}) = \frac{\Delta t}{\alpha}(\mathbf{\Pi}_{\gamma}(\mathbf{u}^{n+1}) + \mathbf{\Pi}_{\gamma}(f_{\mathbf{d}}^n)). \tag{39}$$

If a non-linear constitutive relation is chosen, the same kind of relation is achieved after linearization.

Using again the time discretization of coupling conditions (15) and (19) in (35), we obtain:

$$h_s \int_{\Gamma} \rho_s \alpha \frac{\mathbf{u}^{n+1}}{\Delta t} \cdot \mathbf{v}_s d\Gamma + h_s \frac{\Delta t}{\alpha} \int_{\Gamma} \mathbf{\Pi}_{\gamma}(\mathbf{u}^{n+1} + f_{\mathbf{d}}^n) : \nabla_{\gamma} \mathbf{v}_s d\Gamma = \int_{\Gamma} (-(\sigma_f^{n+1})\mathbf{n} + h_s \rho_s f_{\mathbf{u}}^n) \cdot \mathbf{v}_s d\Gamma, \tag{40}$$

where $\sigma_f^{n+1} = \sigma_f(\mathbf{u}^{n+1}, p^{n+1})$. Eq. (40) is directly embedded in the fluid model. This condition can be seen as a generalized Robin boundary condition involving a stiffness interface matrix that depends on the properties of the arterial wall [29]. Nevertheless we can formally write its *strong* form as a boundary condition for the fluid on the interface Γ:

$$(\sigma_f^{n+1})\mathbf{n} + \frac{h_s \rho_s \alpha}{\Delta t}\mathbf{u}^{n+1} - h_s \frac{\Delta t}{\alpha} \nabla_{\gamma} \cdot \mathbf{\Pi}_{\gamma}(\mathbf{u}^{n+1} + f_{\mathbf{d}}^n) + h_s \frac{\Delta t}{\alpha} H \Pi_{\Gamma}(\mathbf{u}^{n+1} + f_{\mathbf{d}}^n) = h_s \rho_s f_{\mathbf{u}}^n, \tag{41}$$

where $H = \nabla_{\Gamma} \cdot \mathbf{n}$ *is the mean curvature of* Γ. Finally, we present the weak formulation of the reduced order fluid–structure interaction problem. To well define the problem on the interface, we asked for higher regular test functions for the structural problem. Since this model is now written in terms of the fluid velocity, the same degree of regularity has to be ensured now for the test functions of the fluid problem. Choosing transpiration conditions at zero order, let us define the functional space

$$\mathbf{V}_f^{\Gamma} = \{\mathbf{v} \in \mathbf{V}_f : \mathbf{v}|_{\Gamma} \in H^1(\Gamma)\}$$
$$\mathbf{V}_f^{0,\Gamma} = \{\mathbf{v} \in \mathbf{V}_f^0 : \mathbf{v}|_{\Gamma} \in H^1(\Gamma)\}.$$

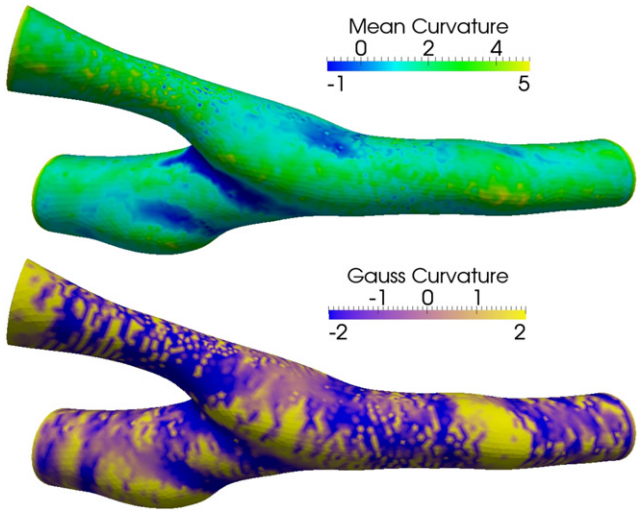

Fig. 3. Reconstructed mean and gauss curvatures on the real geometry of a femoropopliteal bypass.

Fig. 4. Inlet and outlet sections for the post processing of the test case.

The semi-discrete weak formulation of the reduced order FSI problem reads:

for each time step t^n find $(\mathbf{u}^{n+1}, p^{n+1}) \in \mathbf{V}_f^{\Gamma} \times M$ such that:

$$\begin{aligned}
&\int_{\Omega_f} \left(\rho_f \left(\frac{\alpha \mathbf{u}^{n+1}}{\Delta t} + (\mathbf{u}^* \cdot \nabla_x)\mathbf{u}^{n+1} \right) \cdot \mathbf{v} + (\mu(\nabla_x \mathbf{u}^{n+1} + \nabla_x^T \mathbf{u}^{n+1}) - p^{n+1} I) : \nabla_x \mathbf{v} \right) d\Omega_f \\
&\quad + \int_{\Gamma} \left(h_s \rho_s \alpha \frac{\mathbf{u}^{n+1}}{\Delta t} \cdot \mathbf{v} + h_s \frac{\Delta t}{\alpha} \mathbf{\Pi}_\gamma (\mathbf{u}^{n+1} + f_{\mathbf{d}}^n) : \nabla_\gamma \mathbf{v} \right) d\Gamma \\
&= \int_{\Omega_f} (\mathbf{f}_f + \rho_f f_{\mathbf{u}}^n) \cdot \mathbf{v} d\Omega_f + \int_{\Gamma_N} \mathbf{h} \cdot \mathbf{v} d\Gamma + \int_{\Gamma} h_s \rho_s f_{\mathbf{u}}^n \cdot \mathbf{v} d\Gamma \\
&\int_{\Omega} \nabla_x \cdot \mathbf{u} q = 0 \\
&\mathbf{d}^{n+1} = \frac{\Delta t}{\alpha} (\mathbf{u}^{n+1} + f_{\mathbf{d}}^n) \quad \text{on } \Gamma, \qquad \forall (\mathbf{v}, q) \in \mathbf{V}_f^{0,\Gamma} \times M, \text{ with } \mathbf{u}^0 = \mathbf{u}_0
\end{aligned} \tag{42}$$

where $\mathbf{u}^*$ is chosen equal to $\mathbf{u}^{n+1}$ in the case of an implicit treatment of the fluid convective term and it is equal to $\mathbf{u}^n$ in the case of a semi-implicit treatment.

Remark. The extra regularity required on the border Γ is necessary to ensure that the following integral exists:

$$\int_{\Gamma} h_s \frac{\Delta t}{\alpha} \mathbf{\Pi}_\gamma (\mathbf{u}^{n+1}) : \nabla_\gamma \mathbf{v} d\Gamma. \tag{43}$$

The Galerkin finite element formulation of (42) requires the definition of suitable finite element spaces where the solution and test functions are defined. Let us introduce a stable couple of piecewise finite element spaces for velocity and pressure

$$\mathbf{V}_h \subset \mathbf{V}_f^{\Gamma}, \qquad M_h \subset M.$$

If we define $(\mathbf{u}_h^{n+1}, p_h^{n+1}) \in \mathbf{V}_h \times M_h$, $\mathbf{v}_h \in \mathbf{V}_f^{0,\Gamma} \cap \mathbf{V}_h$, and $q_h \in M_h$ then the discrete weak formulation reads exactly as in (42) with $(\mathbf{u}^{n+1}, p^{n+1}) = (\mathbf{u}_h^{n+1}, p_h^{n+1})$ and $(\mathbf{v}, q) = (\mathbf{v}_h, q_h)$.

Remark. A standard finite element space $\mathbf{V}_h$ is indeed a subset of $\mathbf{V}_f^{\Gamma}$ without the need of any enrichment. In fact the trace on Γ of a finite element function $\mathbf{v}_h$ is also a finite element function on the 2D curvilinear manifold Γ, therefore, if we choose zero order transpiration conditions, we directly get $\mathbf{v}_h|_{\Gamma} \in H^1(\Gamma)$.

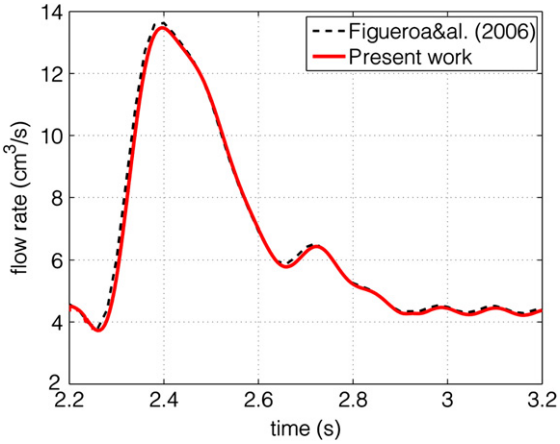

Fig. 5. Flow rate at the section S_1 of the cylinder.

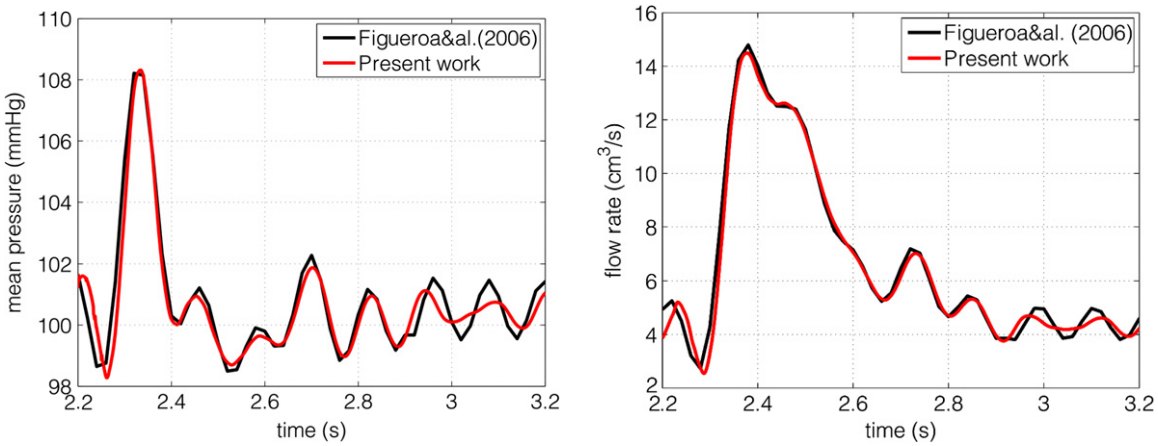

(a) Inlet mean pressure.

(b) Outlet flow rate.

Fig. 6. Mean quantities computed at S_1 and S_2 with constant pressure at outflow. Comparison between our results and those in [18].

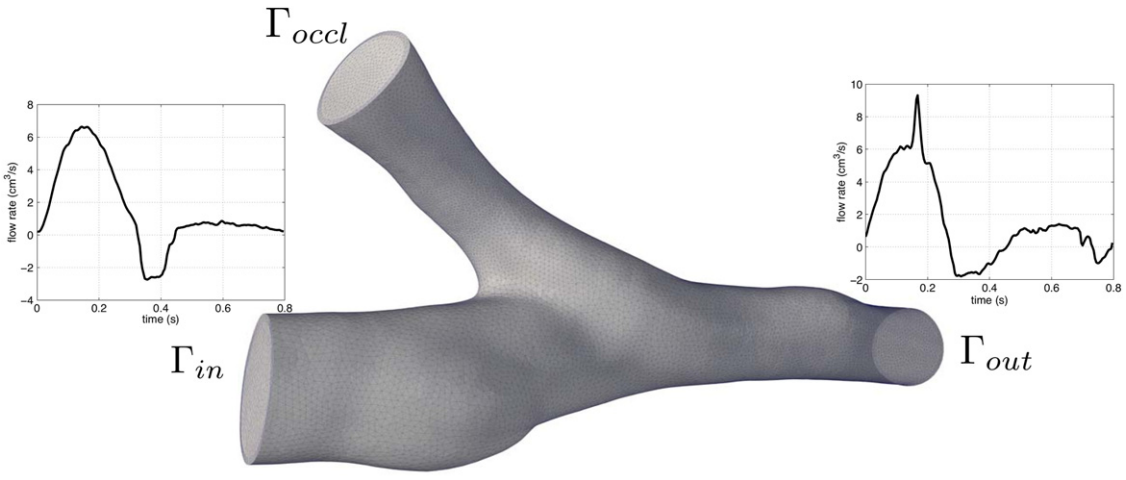

Fig. 7. Femoropopliteal bypass geometry. Graph of the inlet and outlet flow rates, as measured in [36].

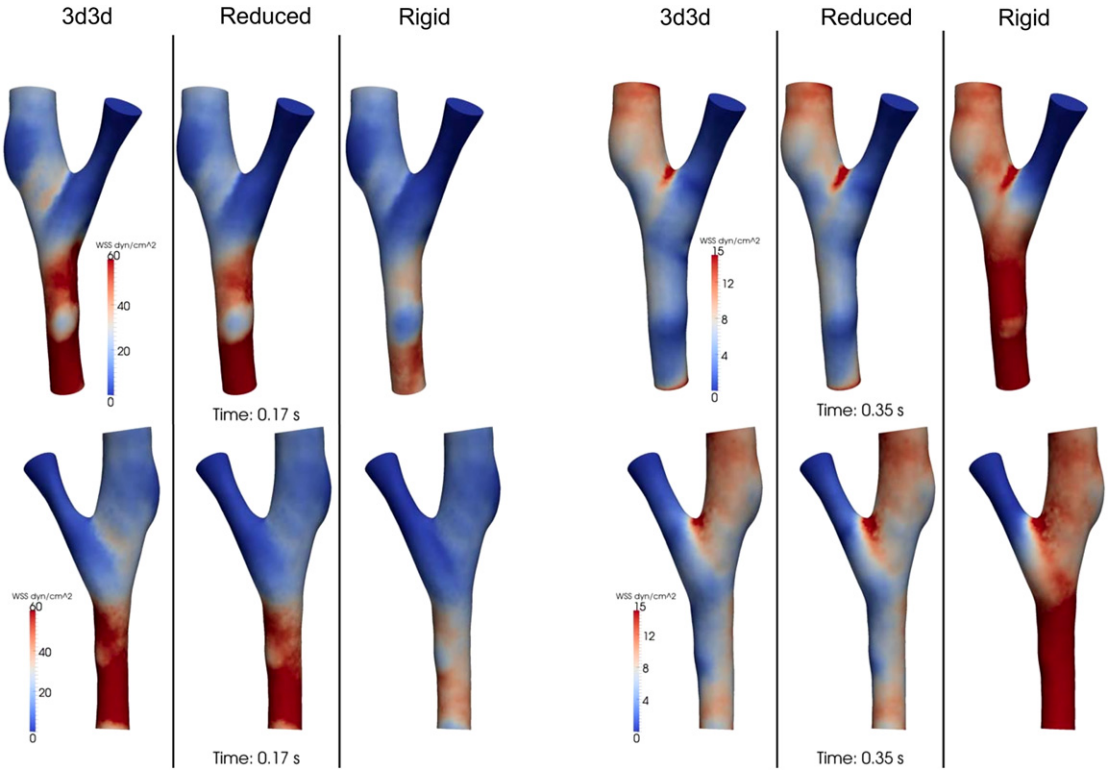

Fig. 8. Comparisons between the pattern of the wall shear stress (dyn/cm^2) at different time steps for different models. On the left: results at time $t = 0.17$ s. On the right: results at time 0.34 s. At the top: back view. At the bottom: front view.

As proposed in [19], we consider a membrane model in the plane stress configuration with an augmented shear stress in the transversal directions. If the coefficient of the transverse shear stress is chosen equal to 1 and considering a linear elastic isotropic constitutive law, $\mathbf{\Pi}_\gamma(\phi)$ reads:

$$\mathbf{\Pi}_\gamma(\phi) = \frac{E}{1+\nu}\frac{\nabla_\gamma\phi + \nabla_\gamma^T\phi}{2} + \frac{E\nu}{1-\nu^2}\nabla_\gamma\cdot\phi. \tag{44}$$

The stress tensor $\mathbf{\Pi}_\gamma$ has been written in terms of the surface gradient $\nabla_\gamma(\cdot)$. From a computational point of view, this formulation is appealing because it does not require the computation of the local rotation matrix for each finite element. In fact, the *surface stiffness* matrix is built using a global approach, by explicitly computing the projection operator of the gradient onto the tangential plane, avoiding the matrix-by-matrix multiplications required to transform the tensor from the Cartesian frame of reference to the normal–tangential one. As it is done in [30], the surface gradient is computed as:

$$\nabla_\gamma\phi = \nabla_x\phi(I - \mathbf{n}\otimes\mathbf{n}), \tag{45}$$

where the symbol $\otimes$ is used for the tensor product and I is the identity operator.

The inertial–algebraic model requires the computation of surface curvature, while the membrane one does not, since the curvature is embedded in the projection operator (the curvature appears in the strong formulation (41) but not in the weak one (40)). Computing the curvature on the surface requires the reconstruction of a P1 field for the normal vector and its derivative. For example, on a real geometry of a femoropopliteal bypass, this process leads to the result shown in Fig. 3 where we note the strong oscillations. Different techniques can be used to yield a smoothed curvature. In the present work, we opted for the reduced order FSI model with the membrane structural equation, avoiding the reconstruction of the curvature. This however requires the implementation of a non-standard boundary condition.

4. Boundary conditions: treatment of the external tissue

Both reduced structural models have been obtained by assuming a zero stress condition on the external boundary of the vessel wall. Nevertheless, it has been shown that in particular cases the constraint of the surrounding tissues cannot be neglected since it leads to the occurrence of non-physiological rigid motions of the vessels. This is e.g. the case of the descending aorta, *linked* to the vertebral bones that bound the movement of the vessel. In a 3D–3D simulation this feature is taken into account by imposing a Robin-like boundary condition on the external boundary of the structure [31,32]. The

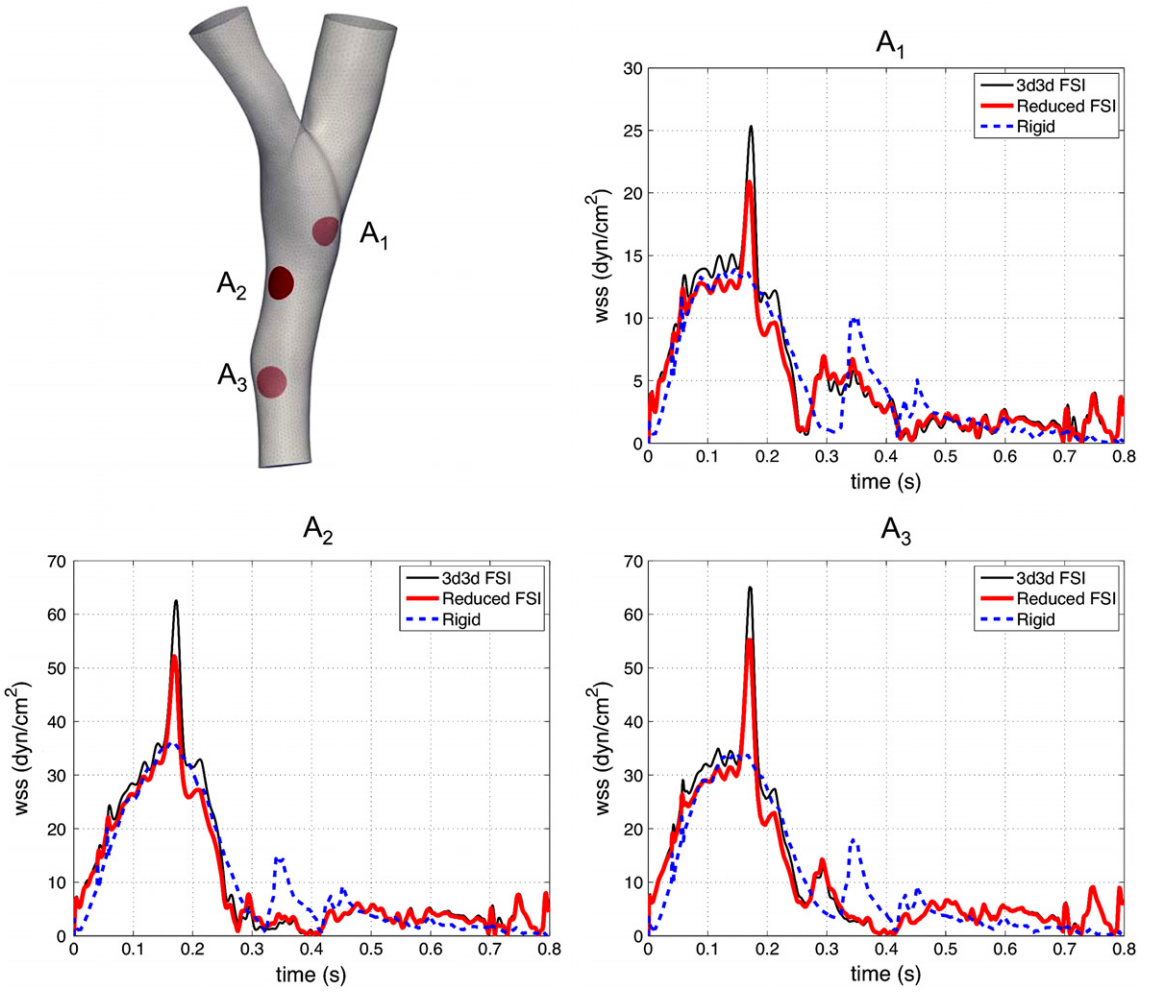

Fig. 9. Mean wall shear stress (dyn/cm^2) in time on three portions of the interface (coarse mesh). In red: reduced order FSI model. In black: 3D–3D FSI model. In blue: Navier–Stokes, rigid walls. (For interpretation of the references to colour in this figure legend, the reader is referred to the web version of this article.)

application of such a boundary condition in a coupled-momentum method was proposed in [31], here we recall how the coefficients of the Robin-like condition change, taking into account the external tissue.

The vessel displacement model reads:

$$\begin{cases} \rho_s \dfrac{\partial^2 \mathbf{d}_s}{\partial t^2} - \nabla_x \cdot \mathbf{\Pi}(\mathbf{d}_s) = \mathbf{0} & \text{in } \Omega_s, \\ \mathbf{d}_s = \mathbf{0} & \text{on } \Gamma^s_{\text{in}} \cup \Gamma^s_{\text{out}}, \\ \mathbf{\Pi}\mathbf{n}_{\text{ext}} + \eta \mathbf{d}_s + \beta \dfrac{\partial \mathbf{d}_s}{\partial t} = \mathbf{0} & \text{on } \Gamma_{\text{ext}}, \end{cases} \tag{46}$$

where on the external boundary a Robin-like boundary condition is imposed as done in [31,32], and η and β depend on the material properties of the surrounding tissue.

The weak formulation of (46) reads:

$$\begin{aligned} &\forall t \in (0, T] \text{ find } \mathbf{d}_s \in L^2(0, T; \mathbf{V}_s) \text{ such that} \\ &\int_{\Omega_s} \rho_s \frac{\partial^2 \mathbf{d}_s}{\partial t^2} \cdot \mathbf{v}_s d\Omega_s + \int_{\Omega_s} \mathbf{\Pi}(\mathbf{d}_s) : \nabla_x \mathbf{v}_s d\Omega_s = \int_{\Gamma} \mathbf{\Pi}(\mathbf{d}_s)\mathbf{n} \cdot \mathbf{v}_s d\Gamma + \int_{\Gamma_{\text{ext}}} \mathbf{\Pi}(\mathbf{d}_s)\mathbf{n}_{\text{ext}} \cdot \mathbf{v}_s d\Gamma_{\text{ext}} \\ &\qquad \forall \mathbf{v}_s \in \mathbf{V}_s, \text{ with } \mathbf{d}_s|_{t=0} = \mathbf{d}_0 \text{ and } \left.\frac{\partial \mathbf{d}_s}{\partial t}\right|_{t=0} = \mathbf{d}_1, \end{aligned} \tag{47}$$

being $\mathbf{d}_0$ and $\mathbf{d}_1$ given functions.

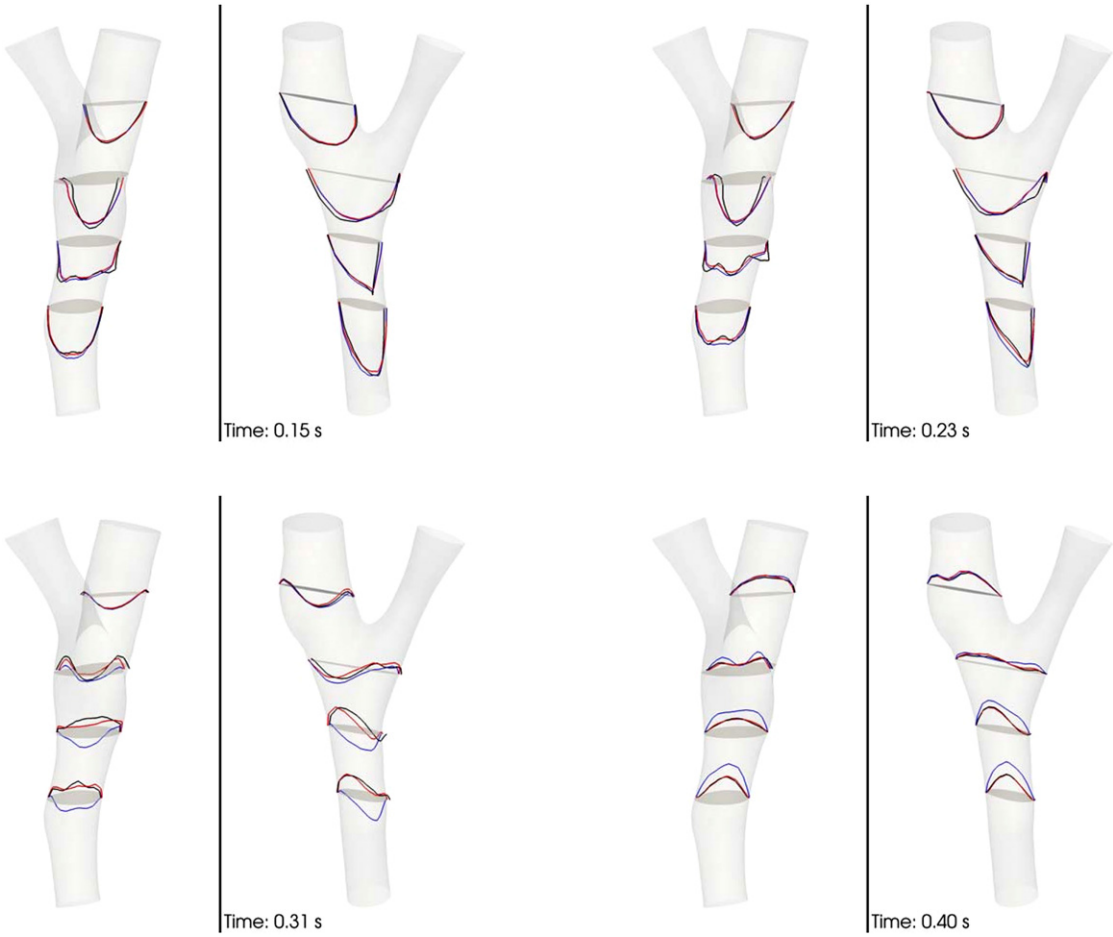

Fig. 10. Section of the velocity profile at different time steps. In red: reduced order FSI model. In black: 3D–3D FSI model. 3D–3D FSI and 3D–3D FSI Transp models are shown only up to 0.6 and 0.5 s, respectively. (For interpretation of the references to colour in this figure legend, the reader is referred to the web version of this article.)

Using the third equation of (46), the integral on Γ_{ext} reads

$$\int_{\Gamma_{\text{ext}}} \mathbf{\Pi}(\mathbf{d}_s)\mathbf{n}_{\text{ext}} \cdot \mathbf{v}_s d\Gamma_{\text{ext}} = -\int_{\Gamma_{\text{ext}}} \left(\eta \mathbf{d}_s + \beta \frac{\partial \mathbf{d}_s}{\partial t}\right) \cdot \mathbf{v}_s d\Gamma_{\text{ext}}. \tag{48}$$

As done in the previous section, thanks to the thin wall approximation ($\Gamma_{\text{ext}} \approx \Gamma$), all the integrals on Ω_s can be expressed as integrals on the interface Γ (multiplied by the thickness h_s). Moreover, using the continuity of the velocities at the interface and the discretization of the temporal derivatives ($\mathbf{d}_s^{n+1} = \frac{\Delta t}{\alpha}(\mathbf{u}^{n+1} + f_{\mathbf{d}}^n)$), the following equation holds:

$$\begin{aligned}\int_{\Gamma} \mathbf{\Pi}(\mathbf{d}_s^{n+1})\mathbf{n}_{\text{ext}} \cdot \mathbf{v}_s d\Gamma_{\text{ext}} &= -\int_{\Gamma} \left(\eta \mathbf{d}_s^{n+1} + \beta \mathbf{u}^{n+1}\right) \cdot \mathbf{v}_s d\Gamma \\ &= -\int_{\Gamma} \left(\eta \frac{\Delta t}{\alpha}(\mathbf{u}^{n+1} + f_{\mathbf{d}}^n) + \beta \mathbf{u}^{n+1}\right) \cdot \mathbf{v}_s d\Gamma. \end{aligned} \tag{49}$$

With this new condition, Eq. (40) is modified as follows:

$$\begin{aligned}&\int_{\Gamma} \left(\frac{h_s \rho_s \alpha}{\Delta t} + \eta \frac{\Delta t}{\alpha} + \beta\right) \mathbf{u}^{n+1} \cdot \mathbf{v}_s d\Gamma + h_s \frac{\Delta t}{\alpha} \int_{\Gamma} \mathbf{\Pi}_{\gamma}(\mathbf{u}^{n+1} + f_{\mathbf{d}}^n) : \nabla_{\gamma} \mathbf{v}_s d\Gamma \\ &= \int_{\Gamma} (-\sigma_f(\mathbf{u}^{n+1}, p^{n+1})\mathbf{n} + h_s \rho_s f_{\mathbf{u}}^n) \cdot \mathbf{v}_s d\Gamma - \int_{\Gamma} \eta \frac{\Delta t}{\alpha} f_{\mathbf{d}}^n \cdot \mathbf{v}_s d\Gamma. \end{aligned} \tag{50}$$

With respect to (40), we are adding here two coefficients to the boundary mass integral of the Robin-like condition that increase the constraint on the interface as the magnitude of η and β increases.

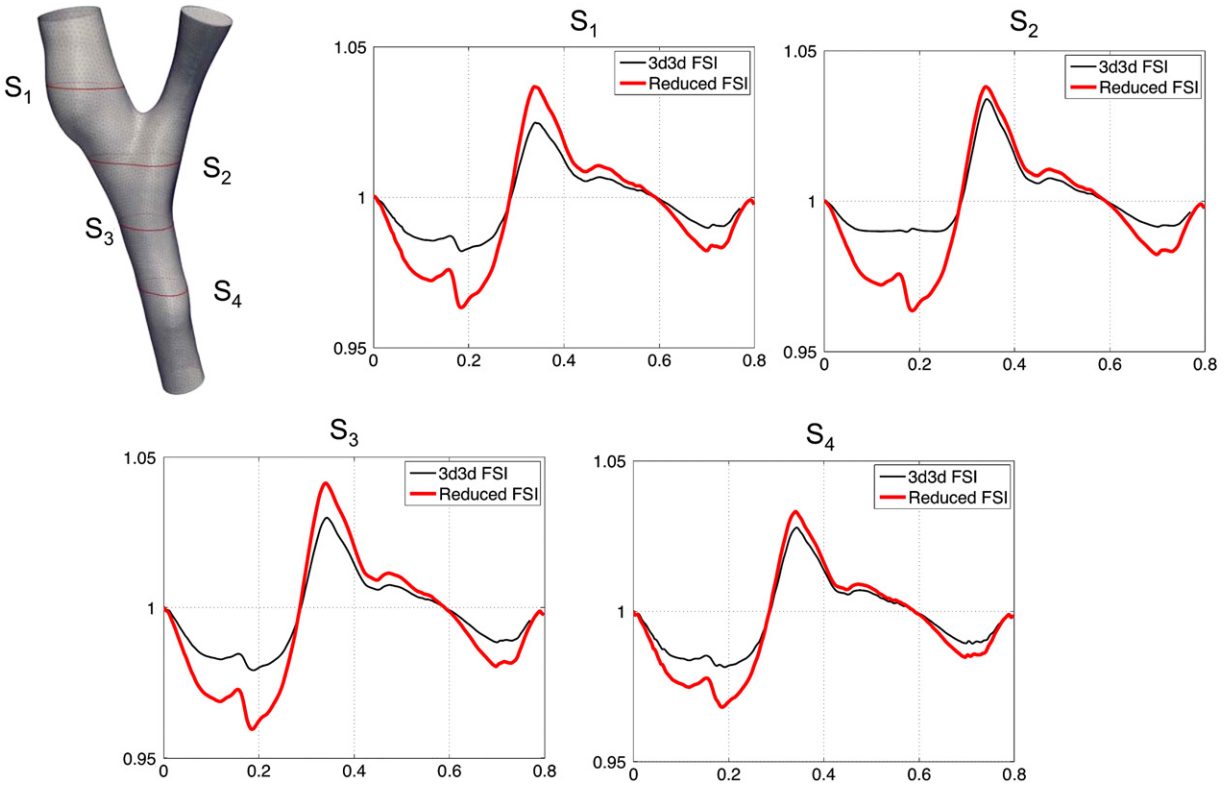

Fig. 11. Relative perimeter in time computed for four slices (coarse mesh). In red: reduced order FSI model. In black: 3D–3D FSI model. 3D–3D FSI and 3D–3D FSI Transp models are shown only up to 0.6 and 0.5 s, respectively. (For interpretation of the references to colour in this figure legend, the reader is referred to the web version of this article.)

5. Comparisons between 3D–3D FSI and reduced order models

In this section we present simulations for three different applications: the first one is a test case on a cylinder and its aim is to validate our code with the results of [18]; the second and the third cases refer to realistic flows and for both of them we compare the results obtained with the membrane model with the ones of a 3D–3D FSI model. For the implementation we used the LifeV library [33] and we choose a finite element discretization P1–P1 with interior penalty stabilization in space [34,35]. In time we use BDF2 for the validation case and implicit Euler scheme for the realistic applications. The convective term of Navier–Stokes is treated semi-implicitly, in all the cases.

The simulations were run on the following parallel supercomputers: **Antares**, a cluster of 56 bi-processors Intel Xeon Nehalem nodes of EPFL, **Cray XT6** HECToR of the UK National Supercomputing Service, and **Cray XE6** Rosa of the Swiss National Supercomputing center, in Lugano.

5.1. Test case: validation on a cylindrical geometry

In the first test case we reproduce the same configuration studied obtained in [18], with the aim of comparing the different models presented so far. We consider a cylinder of diameter 0.6 cm and length 12.6 cm. The thickness of the wall is fixed to 0.03 cm. The Poisson coefficient and the Young modulus of the structure are respectively set to 0.5 and $4.07 \cdot 10^6$ dyn/cm^2. The densities of the vessel wall and of the blood are taken equal to 1.0 g/cm^3 and 1.06 g/cm^3. We consider a Newtonian fluid with constant viscosity equal to 0.04 dyn/cm^2. We truncate the pipe at the section S_1 (Fig. 4) and we impose at S_1 a Dirichlet condition for the velocity using a parabolic profile. This profile is reconstructed to match the flow rate showed in Fig. 5, obtained by the interpolation of the data retrieved from [18]. At the outlet we impose a constant pressure condition. We compute the inlet mean pressure and the outlet flow rate and we compare the results with those in [18].

The results obtained are close to the ones presented in [18] (see Fig. 6). We observe some differences in the final part of the cycle, which could be related to the different choice for the time discretization. Indeed we use a BDF scheme of the second order, whereas, in [18] they use a generalized-α method. Moreover, the inlet condition is not exactly the same, since we retrieve the data for our simulation from a sample of the results presented in [18]. Further validation test cases are ongoing.

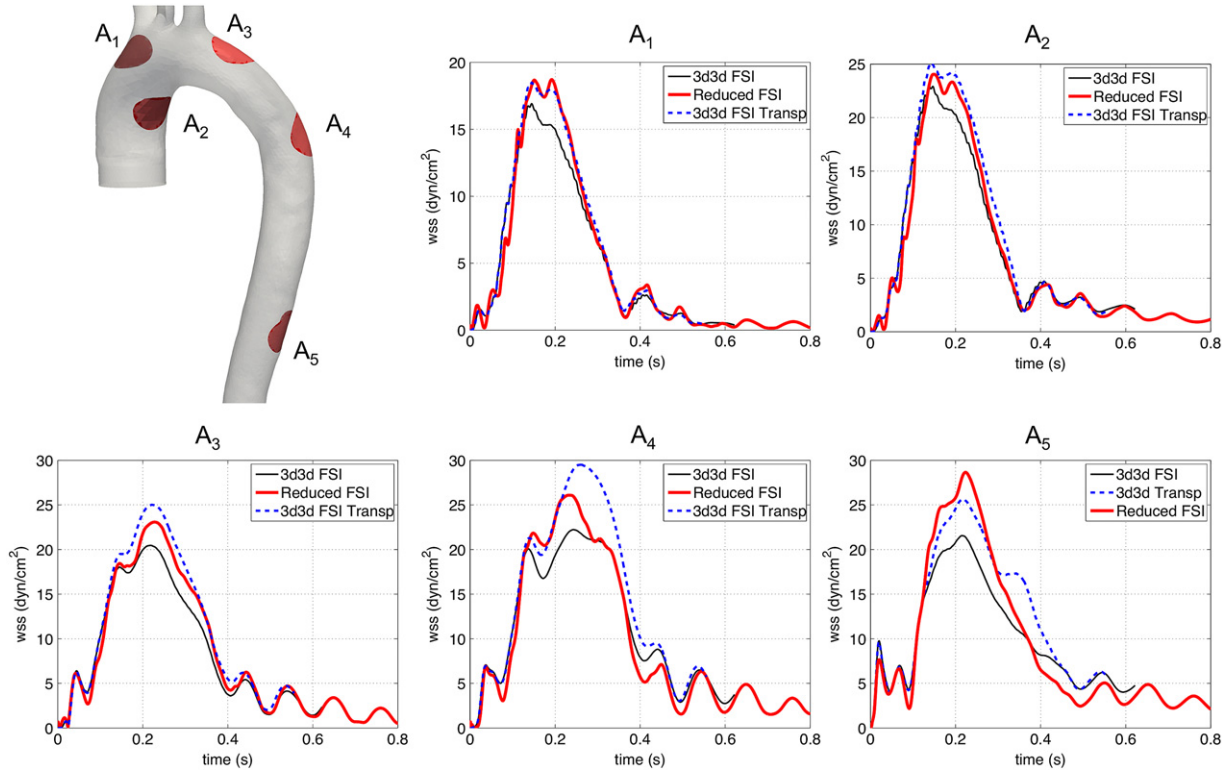

Fig. 12. Mean wall shear stress (dyn/cm^2) in time on five portions of the interface. In red: reduced order FSI model. In black: 3D–3D FSI model. In blue: 3D–3D FSI model with transpiration conditions. (For interpretation of the references to colour in this figure legend, the reader is referred to the web version of this article.)

5.2. Femoropopliteal bypass

In this section we present some results obtained with the membrane model (Section 3.3) applied to the realistic case of a femoropopliteal bypass. The geometry and meshes used are the same considered in [36]. The viscosity of the blood is set to 0.035 P and the density to 1.0 g/cm^3. For the solid part, the Young modulus is 4e6 dyn/cm^2, the Poisson coefficient is 0.45 and the density is 1.2 g/cm^3. The thickness is constant and equal to 0.05 cm. In the case of the femoropopliteal bypass we do not need any enhanced stiffness coming from the external wall, thus we impose a homogeneous Neumann boundary condition. At the inlet and outlet sections we impose flow rates measured on a patient [36] (cf. Fig. 7) and we compare the results with a 3D–3D FSI model and with a Navier–Stokes model where we consider a rigid wall. For the rigid wall case we cannot impose different values of the flow rates at the inlet and at the outlet sections, for this reason on the outlet we impose the pressure that we obtained from the 3D–3D FSI model. The focus is on the behaviour at the interface between the fluid and the solid parts, which, in our case, is represented by the lateral surface of the fluid domain. We compute the wall shear stress on the surface Γ on a mesh made of 48,177 vertices and with 260,554 tetrahedra, the mesh presents a boundary layer on the interface Γ. The presence of the grid boundary layer is important to have an accurate resolution of what is happening near our region of interest.

In Fig. 8 we plot the distribution of the wall shear stress at the time $t = 0.17$ s and $t = 0.35$ s for the 3D–3D FSI model, the reduced order FSI and the rigid case. The pattern of the wall shear stress is similar for the 3D–3D FSI and the reduced order model. Instead, the results obtained with a rigid wall differs significantly from the first two cases.

We show in Fig. 9 the distribution with respect to time of the mean in space of the wall shear stresses on three different portions of the interface. In red we plot the results obtained with the reduced structural membrane model, in black the ones obtained with the 3D–3D FSI model and in blue the results of the rigid case. As we already noted, the 3D–3D FSI and the reduced order models are close, even if, in the reduced order case, the magnitude of the wall shear stress at the systolic peak is lower than the magnitude computed with the fully 3D model. The distribution obtained with rigid walls differs significantly from the other results, in particular during the diastolic phase. In Fig. 10 we report the projection of the velocity profile on two planes at different sections of the domain. The reduced order FSI model is represented in red, the 3D–3D FSI model in black and the rigid wall case in blue. The reduced order model is close to the 3D–3D FSI one and it differs significantly from the rigid case.

From a clinical standpoint, if the critical region of the wall are identified through the value of the wall shear stress, the results of Fig. 8 probably leads to the same considerations for the case of the reduced order model and the 3D–3D FSI one. The

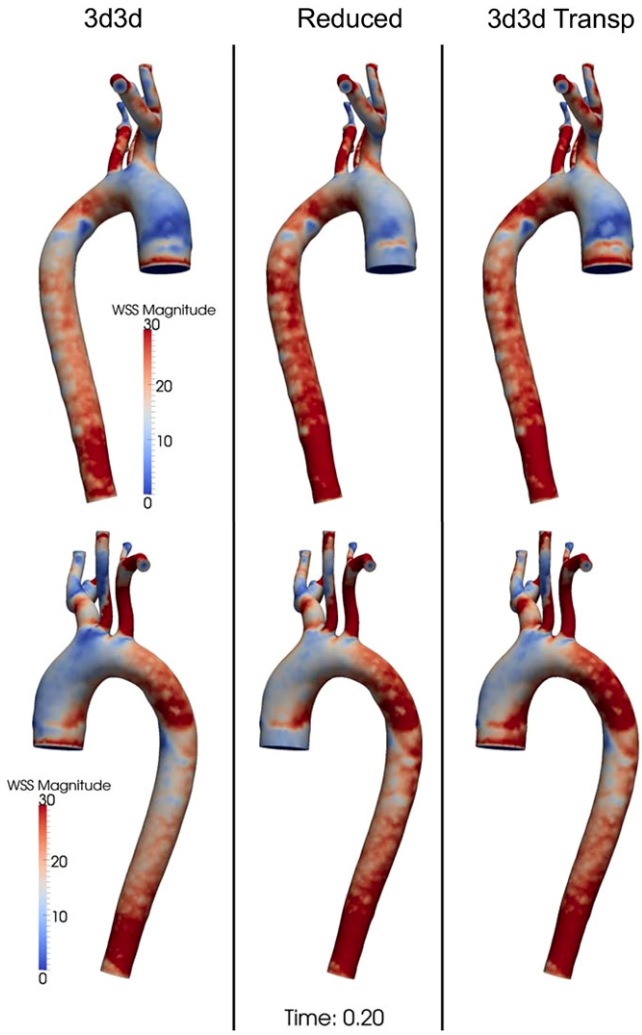

Fig. 13. Pattern of the wall shear stress (dyn/cm^2) near the systolic peak at time $t = 0.2$ s. At the top: back view. At the bottom: front view.

largest mismatch between these two models happens at the systolic peak both for the values of the wall shear stresses and the perimeters (see Fig. 11). One possible way to improve the results could be the use of first order transpiration conditions.

5.3. Aorta

The second case that we address is the flow in an aorta under physiological conditions. The physical parameters for both the blood and the solid wall are the same as for the femoropopliteal bypass case. We impose patient-specific flow rates at each outflow boundary [37]. At the ascending aorta inlet section a Dirichlet boundary condition in the normal direction is imposed in order to match the experimental flow rate. On the external wall of the structure we impose a Robin boundary condition as in (46) with coefficient $\beta = 0$ and $\eta = 9e4$ for the small branches and $\eta = 6e4$ elsewhere [32]. For the fluid domain discretization, we use a mesh with 114,660 vertices and 837,502 tetrahedra. The reduced order FSI model discretized with P1–P1 stabilized finite elements in space is then composed of 578,640 degrees of freedom. For the 3D–3D FSI model, we have to add 251,485 degrees of freedom (80,495 vertices) of the solid domain. The mesh features a boundary layer at the interface between fluid and solid and at each inlet/outlet boundary a flow extension is added in order to obtain a circular inlet/outlet section [38].

We compare three models: 3D–3D FSI, 3D–3D FSI with transpiration conditions at the zero order and reduced order FSI model with the membrane assumption, again with zero order transpiration conditions. In Figs. 12 and 13 we display the mean wall shear stress on five different portions of the interface and the pattern of the wall shear stress near the systolic peak. In Figs. 14 and 15, the velocity profiles at different time steps and the percentage of variation of the perimeters for five different slices are showed.

We recall that we obtained the reduced order FSI model based on two *levels* of reduction: the application of the transpiration conditions and the membrane assumption with the consequent embedding of the structure inside the Navier–Stokes

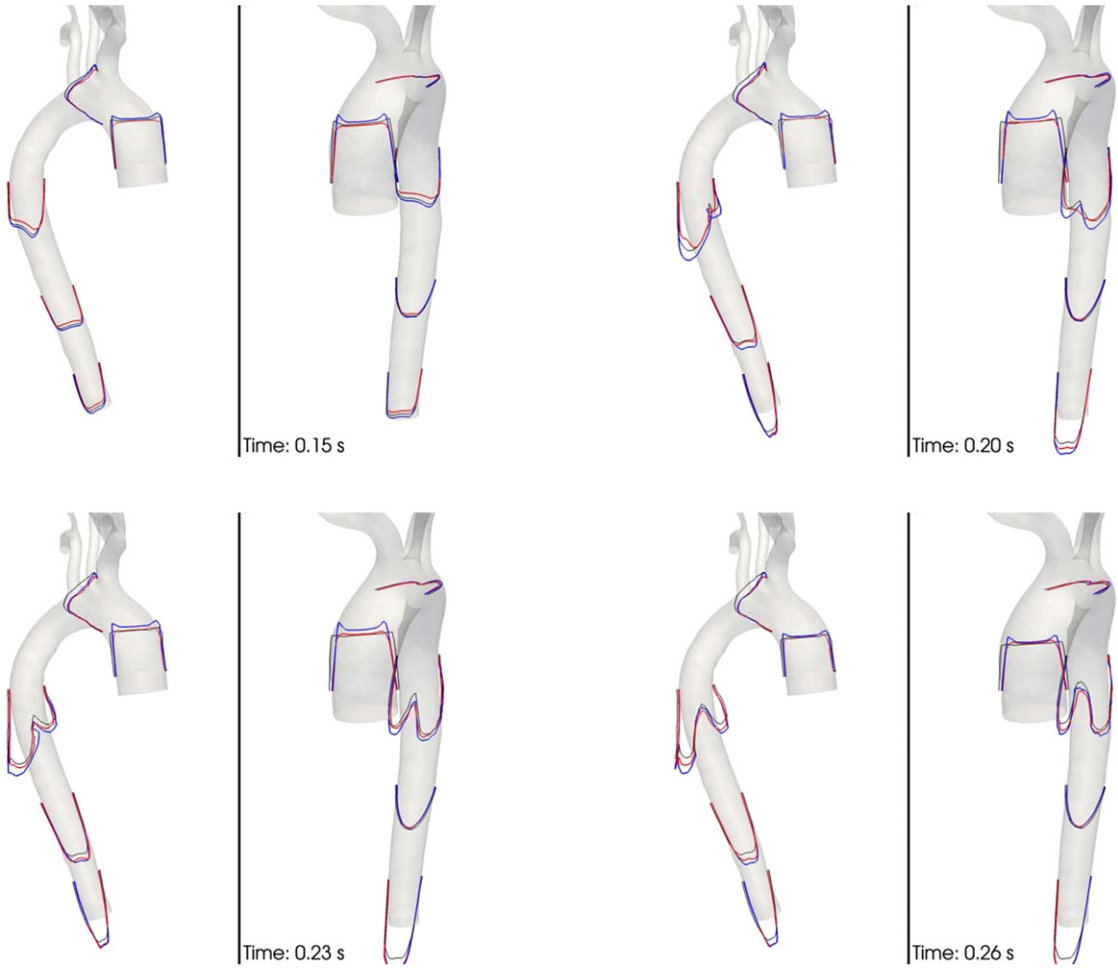

Fig. 14. Velocity profiles at five different sections of the geometry. In red: reduced order FSI model. In black: 3D–3D FSI model. In blue: 3D–3D FSI model with transpiration conditions. (For interpretation of the references to colour in this figure legend, the reader is referred to the web version of this article.)

system under the form a boundary condition. The difference between the 3D–3D FSI and the reduced order model can be formally examined by looking at two contributions: we first analyse the effects of the transpiration conditions and then those of the structural model reduction.

From Figs. 12 and 15 we notice that, during the first 0.15 s of the cardiac cycle, the three models are overlapping. Then, near the systolic peak (0.2 s ca), there are regions (areas A_1, A_2 and A_3 of Fig. 12) where the gap between the 3D–3D FSI and the reduced order FSI model is mainly due to the linearization of the domain position. Indeed, the values of the mean wall shear stress of the 3D–3D FSI model with transpiration conditions and the reduced order one are overlapped, while values of the wall shear stress of the fully 3D–3D FSI is lower. This is visible also from Fig. 13, where the pattern of the wall shear stresses of the 3D–3D transpiration and the reduced order model are similar. After the systolic peak, the values of the wall shear stress measured with 3D–3D transpiration model realign with the values of the 3D–3D FSI one, while the stresses computed with the reduced order model are lower in the case of areas A_4 and A_5. In Fig. 15 it is clear that, even if in the 3D–3D transpiration model the mesh is fixed, the values of the displacement computed by the model is close to the values computed with the 3D–3D FSI one. On the contrary, the displacements of the reduced order model are lower and, even if the curves present the same shape, the approximation of the structure to a membrane seems to produce a loss of load. The results presented so far are obtained initializing the simulation using zero values for all the variables. The results of Fig. 15 shows the importance of a reinitialization of the membrane model with the end-diastolic pre-stressed that differs from the end-diastolic pre-stressed of the 3D–3D FSI model.

6. Conclusions

In this work we have compared a reduced order FSI model (the coupled momentum method) and 3D–3D FSI models (with and without transpiration conditions) on two patient-specific cases: a femoropopliteal bypass and an aorta in physiological

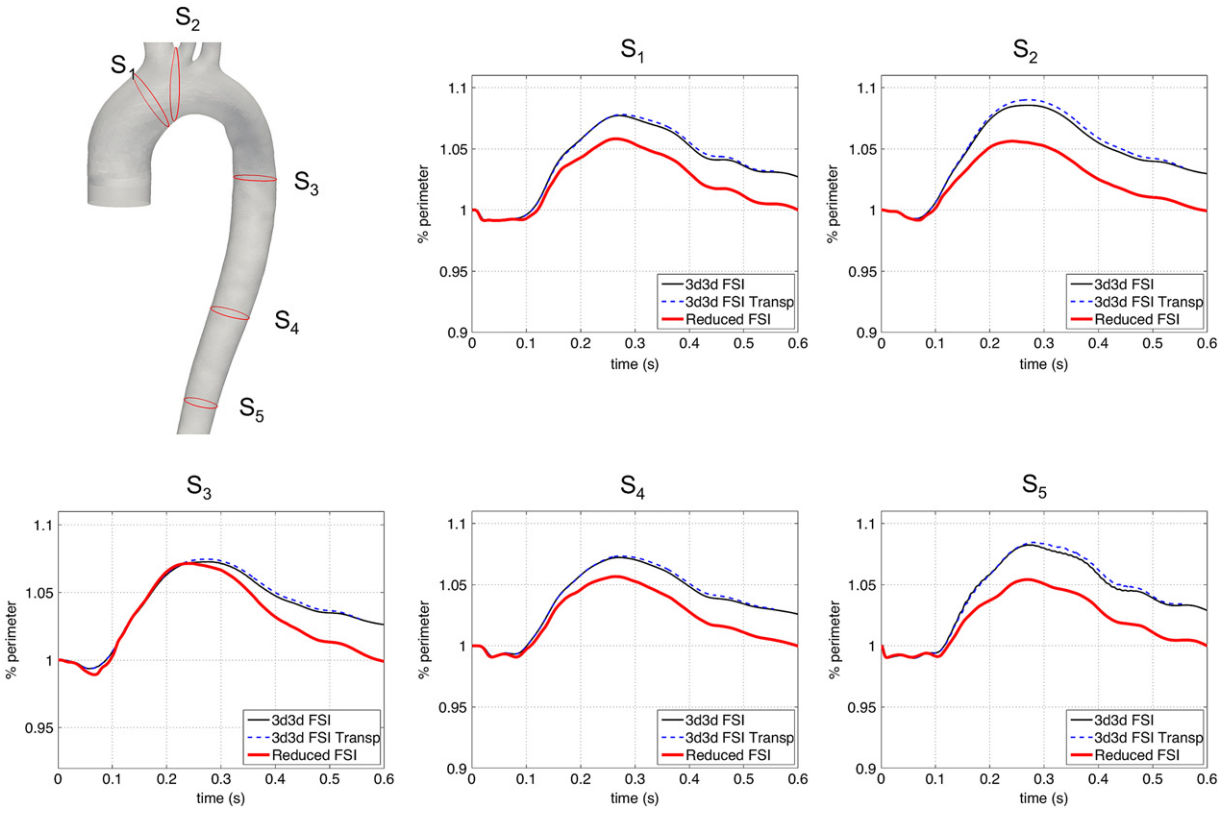

Fig. 15. Relative measures of the perimeters of five different slices of the domain. In red: reduced order FSI model. In black: 3D–3D FSI model. In blue: 3D–3D FSI model with transpiration conditions. (For interpretation of the references to colour in this figure legend, the reader is referred to the web version of this article.)

conditions. In the case of the femoropopliteal bypass the results, in terms of wall shear stresses, obtained with the reduced order model are close to the 3D–3D FSI ones. The coupled momentum method without a retuning of the parameters is then worth to be used in those specific applications where the assumption of small displacement holds, as it is done in several works [39,18,31,19,40], for other biomedical applications.

When dealing with the simulation of the flow in the aorta, the displacement and the forces in play are much larger. Here, the differences between the reduced models and the 3D–3D FSI one is more accentuated. In terms of percentage, the variation of the radius is less than 5% for the bypass case and below 8% for the aorta one. However, in absolute value is about 0.025 cm for the bypass and 0.15 cm in the aorta. Since the modelling error related to the transpiration conditions is of order $O(\|\widehat{\mathbf{d}}_s|_{\widehat{\Gamma}}\|)$ (see Eq. (14)), this means that in the aorta is one order of magnitude larger than in the bypass. One possible solution to improve the results without updating the mesh at each time step could be to use transpiration conditions at first order.

Another important future development of this work will concern the evaluation of the distance of the numerical results from the experimental *in-vivo* data and its comparison with the differences between the 3D–3D FSI and the reduced models.

Acknowledgements

We thank Jean Bonnemain, Elena Faggiano, and Emilie Sauvage for their contribution in the mesh generation in the realistic cases and Professor C.A. Figueroa for sharing his results for the validation test case. We would like to thank also Paolo Crosetto for the support for 3D–3D FSI simulations. Acknowledgements to the LifeV community, the Swiss Center for Scientific Computing for the support and the computing resources, and to the European Research Council Advanced Grant, Mathcard, Mathematical Modelling and Simulation of the Cardiovascular System, Project ERC-2008-AdG 227058.

References

[1] L. Formaggia, A. Quarteroni, A. Veneziani, Cardiovascular Mathematics, Springer, 2009.
[2] W.W. Nichols, M.F. O'Rourke, McDonald's Blood Flow in Arteries—Theoretical, Experimental and Clinical Principles, Arnold, 1998.
[3] L. Formaggia, F. Nobile, A. Quarteroni, A. Veneziani, Multiscale modelling of the cirulatory system: a preliminary analysis, Computing and Visualization in Science 2 (2–3) (1999) 75–83.
[4] A. Malossi, P. Blanco, S. Deparis, A two-level time step technique for the partitioned solution of one-dimensional arterial networks, Computer Methods in Applied Mechanics and Engineering 237–240 (2012) 212–226.

[5] J. Gerbeau, M. Vidrascu, A quasi-Newton algorithm based on a reduced model for fluid–structure interaction problems in blood flows, M2AN Mathematical Modelling and Numerical Analysis 37 (4) (2003) 663–680.
[6] S. Deparis, M.A. Fernandez, L. Formaggia, Acceleration of a fixed point algorithm for fluid–structure interaction using transpiration conditions, M2AN Mathematical Modelling and Numerical Analysis 37 (4) (2003) 601–616.
[7] S. Deparis, M. Discacciati, A. Quarteroni, A domain decomposition framework for fluid–structure interaction problems, in: Proceedings of the Third International Conference on Computational Fluid Dynamics, ICCFD3, 2006, pp. 41–58.
[8] S. Deparis, M. Discacciati, G. Fourestey, A. Quarteroni, Fluid–structure algorithms based on Steklov–Poincaré operators, Computer Methods in Applied Mechanics and Engineering 195 (41–43) (2006) 5797–5812.
[9] A. Quaini, A. Quarteroni, A semi-implicit approach for fluid–structure interaction based on an algebraic fractional step method, Mathematical Models and Methods in Applied Sciences 17 (6) (2007) 957–983.
[10] S. Badia, A. Quaini, A. Quarteroni, Splitting methods based on algebraic factorization for fluid–structure interaction, SIAM Journal on Scientific Computing 30 (4) (2008) 1778–1805.
[11] S. Badia, A. Quaini, A. Quarteroni, Modular vs. non-modular preconditioners for fluid–structure systems with large added-mass effect, Computer Methods in Applied Mechanics and Engineering 197 (49–50) (2008) 4216–4232.
[12] F. Nobile, C. Vergara, An effective fluid–structure interaction formulation for vascular dynamics by generalized robin conditions, SIAM Journal on Scientific Computing 30 (2) (2008) 731–763.
[13] S. Canic, J. Tambaca, G. Guidoboni, A. Mikelic, C. Hartley, D. Rosenstrauch, Modeling viscoelastic behaviour of arterial walls and their interaction with pulsatile blood flow, SIAM Journal on Applied Mathematics 67 (1) (2006) 164–194.
[14] G. Guidoboni, R. Glowinski, N. Cavallini, S. Canic, Stable loosely-coupled-type algorithm for fluid–structure interaction in blood flow, Journal of Computational Physics 228 (18) (2009) 6916–6937.
[15] G. Guidoboni, R. Glowinski, N. Cavallini, S. Canic, S. Lapin, A kinematically coupled time-splitting scheme for fluid–structure interaction in blood flow, Journal of Computational Physics 22 (5) (2009) 684–688.
[16] M. Bukac, S. Canic, R. Glowinski, J. Tambaca, A. Quaini, Fluid–structure interaction in blood flow capturing non-zero longitudinal structure displacement, Journal of Computational Physics 235 (2012) 515–541.
[17] M.A. Fernandez, Incremental displacement-correction schemes for incompressible fluid–structure interaction, Numerische Mathematik (2012) http://dx.doi.org/10.1007/s00211-012-0481-9.
[18] C.A. Figueroa, I.E. Vignon-Clementel, K.E. Jansen, T.J. Hughes, C.A. Taylor, A coupled momentum method for modeling blood flow in three-dimensional deformable arteries, Computer Methods in Applied Mechanics and Engineering 195 (41–43) (2006) 5685–5706.
[19] C.A. Figueroa, S. Baek, C.A. Taylor, J.D. Humphrey, A computational framework for fluid–solid-growth modeling in cardiovascular simulations, Computer Methods in Applied Mechanics and Engineering 198 (45–46) (2009) 3583–3601.
[20] G. Rozza, Shape design by optimal flow control and reduced basis techniques: application to bypass configurations in haemodynamics, Ph.D. Thesis, École Polytechnique Fédérale de Lausanne, 2005.
[21] A. Quarteroni, G. Rozza, A. Manzoni, Certified reduced basis approximation for parametrized partial differential equations and applications, Journal of Mathematics in Industry 1 (3) (2011) http://dx.doi.org/10.1186/2190-5983-1-3.
[22] A. Manzoni, A. Quarteroni, G. Rozza, Shape optimization for voscous flows by reduced basis methods and free-form deformation, International Journal for Numerical Methods in Fluids 70 (2012) 646–670.
[23] A. Manzoni, Reduced models for optimal control, shape optimization and inverse problems in haemodynamics, Ph.D. Thesis, EPFL, 2012.
[24] T.J. Hughes, W. Liu, T. Zimmermann, Lagrangian–Eulerian finite element formulation for incompressible viscous flow, Computer Methods in Applied Mechanics and Engineering 29 (1981) 329–349.
[25] J. Donea, S. Giuliani, J. Halleux, An arbitrary Lagrangian–Eulerian finite element method for transient dynamic fluid–structure interaction, Computer Methods in Applied Mechanics and Engineering 33 (1982) 689–723.
[26] M.A. Fernandez, J. Gerbeau, C. Grandmont, A projection semi-implicit scheme for the coupling of an elastic structure with an incompressible fluid, International Journal for Numerical Methods in Engineering 64 (4) (2007) 794–821.
[27] P. Crosetto, S. Deparis, G. Fourestey, A. Quarteroni, Parallel algorithms for fluid–structure interaction problems in haemodynamics, SIAM Journal on Scientific Computing 33 (4) (2011) 1598–1622.
[28] A. Porpora, P. Zunino, C. Vergara, M. Piccinelli, Numerical treatment of boundary conditions to replace lateral branches in haemodynamics, International Journal for Numerical Methods in Biomedical Engineering (2012) http://dx.doi.org/10.1002/cnm.2488.
[29] L. Gerardo-Giorda, F. Nobile, C. Vergara, Analysis and optimization of Robin–Robin partitioned procedures in fluid–structure interaction problems, SIAM Journal on Numerical Analysis 48 (6) (2012) 2091–2116.
[30] A. Bonito, R. Nochetto, M.S. Pauletti, Dynamics of biomembranes: effect of the bulk fluid, Mathematical Modelling of Natural Phenomena 6 (5) (2011) 25–43.
[31] P. Moireau, N. Xiao, M. Astorino, C.A. Figueroa, D. Chapelle, C.A. Taylor, J. Gerbeau, External tissue support and fluid–structure simulation in blood flows, Biomechanics and Modeling in Mechanobiology 11 (1–2) (2012) 1–18.
[32] A. Malossi, J. Bonnemain, Numerical comparison and calibration of geometrical multiscale models for the simulation of arterial flows, Cardiovascular Engineering and Technology 4 (4) (2013) 440–463.
[33] LifeV, A parallel finite element library, 2012. http://www.lifev.org/.
[34] E. Burman, M.A. Fernandez, P. Hansbo, Continuous interior penalty finite element method for Oseen's equations, SIAM Journal on Numerical Analysis 44 (3) (2006) 1248–1274.
[35] E. Burman, M.A. Fernandez, Continuous interior penalty finite element method for the time-dependent Navier–Stokes equations: space discretization and convergence, Numerische Mathematik 107 (1) (2007) 39–77.
[36] E. Marchandise, P. Crosetto, C. Geuzaine, J.-F. Remacle, E. Sauvage, Quality open source mesh generation for cardiovascular flow simulation, in: D. Ambrosi, A. Quarteroni, G. Rozza (Eds.), Modeling of Physiological Flows, 2011.
[37] P. Crosetto, Fluid–structure interaction problems in hemodynamics: parallel solvers, preconditioners and applications, Ph.D. Thesis, École Polytechnique Fédérale de Lausanne, 2011.
[38] J. Bonnemain, E. Faggiano, A. Quarteroni, S. Deparis, A framework for the analysis of the haemodynamics in patient with ventricular assist device, ePFL MATHICSE Technical Report, 2012.
[39] H.J. Kim, I.E. Vignon-Clementel, J.S. Coogan, C.A. Figueroa, K.E. Jansen, C.A. Taylor, Patient-specific modeling of blood flow and pressure in human coronary arteries, Annals of Biomedical Engineering 38 (10) (2010) 3195–3209.
[40] C.A. Figueroa, C.A. Taylor, V. Yeh, A.J. Chiou, C.K. Zarins, Effect of curvature on displacement forces acting on aortic endografts: a 3-dimensional computational analysis, Journal of Endovascular Therapy 16 (3) (2009) 284–294.